

Hole- and electron-injection driven phase transitions in transition metal dichalcogenides and beyond: A unified understanding

Xiao-Huan Lv, Meng-Qi Wu, Yin-Ti Ren, Rui-Ning Wang,* Hu Zhang, Chen-Dong Jin, Ru-Qian Lian, Peng-Lai Gong, Xing-Qiang Shi,* and Jiang-Long Wang*

Key Laboratory of Optic-Electronic Information and Materials of Hebei Province, Institute of Life Science and Green Development, College of Physics Science and Technology, Hebei University, Baoding 071002, P. R. China

*E-mails: rnwang@hbu.edu.cn; shixq20hbu@hbu.edu.cn; jlwang@hbu.edu.cn

Abstract: The phase transitions among polymorphic two-dimensional (2D) transition metal dichalcogenides (TMDs) have attracted increasing attention for their potential in enabling distinct functionalities in the same material for making integrated devices. Electron-injection to TMDs has been proved to be a feasible way to drive structural phase transition from the semiconducting H-phase to the semimetal dT-phase. In this contribution, based on density-functional theory (DFT) calculations, firstly we demonstrate that hole-injection drives the transition of the H-phase more efficiently to the metallic T-phase than to the semimetallic dT-phase for group VI-B TMDs (MoS_2 , WS_2 , and MoSe_2 , etc.). The origin can be attributed to the smaller work function of the T-phase than that of the dT-phase. Our work function analysis can distinguish the T and dT phases quantitatively while it is challenging for the commonly used crystal field splitting analysis. In addition, our analysis provides a unified understanding for both hole- and electron-injection induced phase transitions for 2D materials beyond TMDs, such as the newly synthesized MoSi_2N_4 family. Moreover, the hole-driven T-phase transition mechanism can explain the recent experiment of WS_2 phase transition by hole-doping with yttrium (Y) atoms. Using 1/3 Y-doped WS_2 and MoSe_2 as examples, we show that the Mo and W valency increases to 5+. These above findings open up an avenue to obtain the metallic T-phase, which expands the possible stable phases of 2D materials.

I. INTRODUCTION

Two-dimensional transition metal dichalcogenides (TMDs) have attracted increasing attention in fundamental research and device applications for their unique structural, physical and chemical properties[1-4]. The group VI-B TMD monolayers, MX_2 ($\text{M} = \text{W}, \text{Mo}$; $\text{X} = \text{S}, \text{Se}, \text{Te}$), have several polymorphs such as the H, T and dT phases[5-7]. In the H structure, the X-M-X atomic layers form AbA stacking (Fig. 1a); while in the T structure, the three atomic layers form AbC stacking (Fig. 1b). The T-phase can be obtained by alkali atom intercalation, and may coexist with the other phases[8]. The isolated T-phase structure is generally unstable and undergoes spontaneous lattice distortion along the x direction (as denoted in Fig. 1c), forming the dT-phase with a doubled ($\sqrt{3} \times 1$) rectangular cell, where the distorted M atoms form one-dimensional zigzag chains in the y direction as indicated by the dashed lines in Fig. 1c[9,10]. For the H-phase TMDs, many have semiconducting properties with spin-orbit coupling and exciton effects for various applications such as field effect transistors[11,12], magnetic tunnel junctions[13], valleytronics[14] and optoelectronics[15-17]. For the T-phase and its distorted form (the dT-phase), large magneto resistance, interesting quantum spin Hall effect[18] and higher catalytic activity[19] have been reported. Recently, the phase engineering and phase transition between polymorphic 2D TMDs have attracted increasing attention for the potential of enabling distinct functionalities in the same material. For example, the integration of H and dT phases in MoTe_2 thin film by laser-induced transition have been shown to be an Ohmic homojunction[20].

Different methods have been reported to induce phase transition from the H- to the dT- or T-phase, such as the intercalation[21] of alkali metal ions Li, Na, and K[22], injection of electrons[23,24], applying stresses[25,26], changing temperature[6,10], laser and focused electron beams[20,27], and doping with transition metal elements[28-32]. A recent theoretical work has demonstrated that electron-injection is a feasible mean to drive structural transition from the semiconducting H-phase to semimetal dT-phase[23], and, recently the hole-injection induced transition to metallic T-phase (not dT) has been realized in the experiment[33]. However, the mechanism of hole-injection induced T-phase transition of TMDs and a unified understanding for both hole- and electron-driven phase transitions in TMDs and beyond remain lack. The possible reason is that it is challenging for the commonly used crystal field splitting analysis to distinguish quantitatively between the T- and dT-phase. New analysis methods are needed.

In the current work, we conducted a systematic density functional theory study to provide a unified understanding to both hole- and electron-injection driven phase transitions of group VI-B TMDs and beyond, and then realized the proposed hole-injection driven phase transition in real systems. We found that hole-injection drives the H-phase transition more efficiently to the metallic T-phase than to the semimetallic dT-phase, and then revealed the phase transition mechanism through an analysis of the different work functions between the different phases. Our simple work function analysis can distinguish the T and dT phases quantitatively. Finally, inspired by the recent experiment[33], we used yttrium (Y)-doped MX_2 to demonstrate the realization of hole-injection driven phase transition in real systems, in which the valency of M atoms increases to 5+ under 1/3 Y concentration.

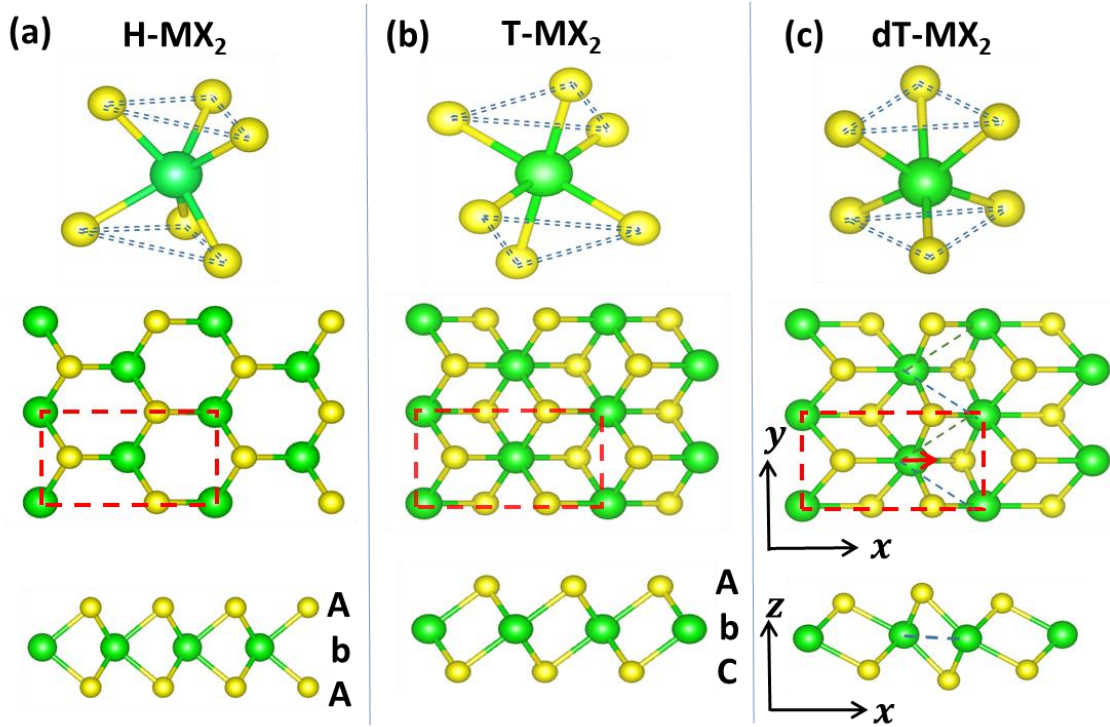


FIG. 1. Atomistic structures of monolayer transition metal dichalcogenides, MX_2 ($\text{M} = \text{Mo}, \text{W}$; $\text{X} = \text{S}, \text{Se}, \text{Te}$), in different phases. (a) 1H-MX₂ in AbA stacking; (b) 1T-MX₂ in AbC stacking; and (c) distorted 1T-MX₂ (dT-MX₂), where the distorted M atoms form one-dimensional zigzag chains as indicated by the dashed lines along the y-direction. Unit cells are indicated by red rectangles; the cell sizes in the H- and T-structure are doubled to compare with the doubled ($\sqrt{3} \times 1$) rectangular cell in the dT-structure.

II. CALCULATION METHODS

Spin-polarized density functional theory calculations were performed using the Vienna *ab initio* Simulation Package (VASP)[34,35] The projector augmented wave (PAW) potentials was adopted to describe the core electrons[36]. The valence electrons were described by plane waves with a cut-off kinetic energy of 400 eV. The electronic exchange-correlation energy was treated by the generalized-gradient approximation of Perdew-Burke-Ernzerhof (GGA-PBE)[37] form. A vacuum layer of ~ 20 Å along the z-direction was added to avoid the spurious interaction between neighboring slabs. The K -point sampling in the Brillouin zone adopts the Monkhorst-Pack scheme with a grid density of $11 \times 11 \times 1$ and $7 \times 11 \times 1$ for 1×1 and $\sqrt{3} \times 1$ cells, respectively. A similar K -point density was used for other calculations. The convergence criteria of energy and forces acting on each atom were 10^{-5} eV and 0.01 eV Å⁻¹, respectively. For bonding analysis, the LOBSTER package was used[38].

III. RESULTS AND DISCUSSIONS

The lattice parameters and electronic band structures of group VI-B TMD monolayers, MX_2 ($\text{M} = \text{Mo}, \text{W}$; $\text{X} = \text{S}, \text{Se}$ and Te), are summarized in Table S1 and Fig. S1 in the Supporting Information. Fig. 2 compares the relative energetic stabilities among the H, T and dT phases, which is the starting point to study the phase transitions among them induced by hole- and electron-injections. The energy differences among the three phases change monotonously with the increase of the period of X atom from S to Se to Te for both MoX_2 and WX_2 . In detail, the energy difference between the T (or dT)-phase and the H-phase, $E(\text{T})-E(\text{H})$ or $E(\text{dT})-E(\text{H})$, decreases as the period of the X atom increases; while the energy difference between T and dT, $E(\text{T})-E(\text{dT})$, increases with the increase of the X atom period. For MoTe_2 , the H and dT phases can coexist in experiment[2], while the stable structure of WTe_2 in experiment is the dT-phase[10,39,40].

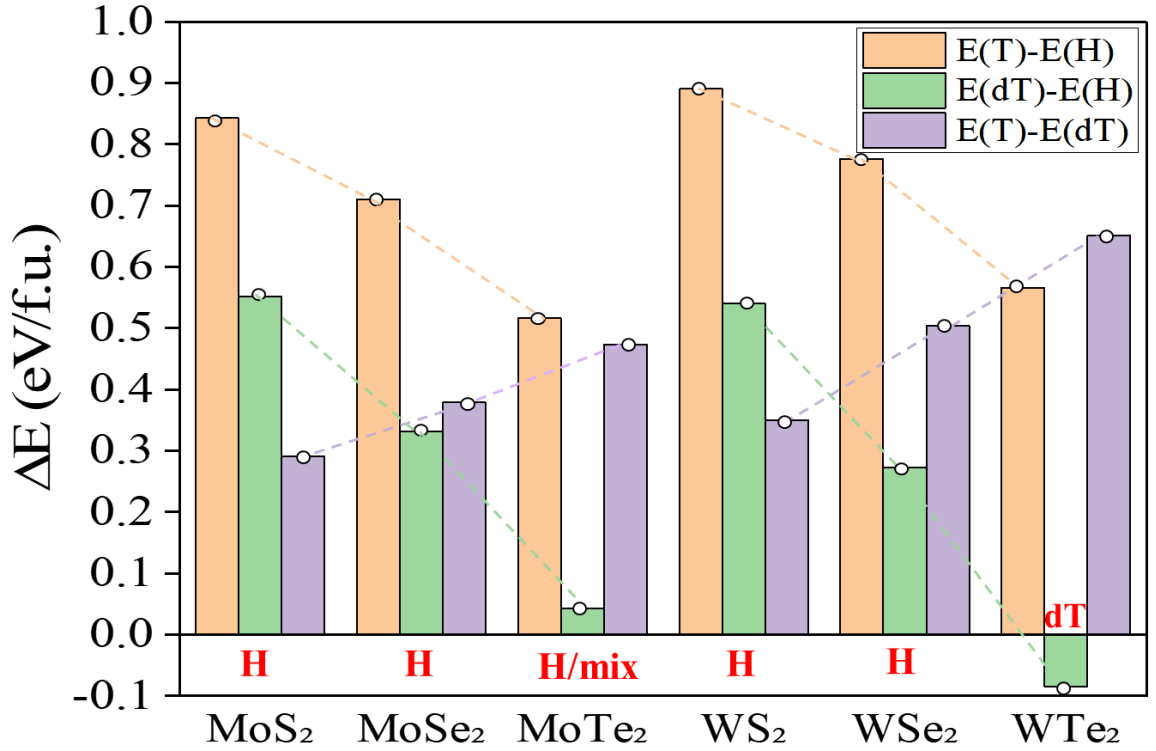


FIG. 2. Energy differences are in units of eV per formula unit (eV/f.u.) among the three phases of group VI-B TMD monolayers. The energy differences change monotonously with the increase of the period of X atom from S to Se to Te for both MoX₂ and WX₂ (see the dashed lines guide the eye). The labeled “H”, “H/mix”, and “dT” in the lower part of the figure denotes the stable structure in experiment is the H-phase, the mixed H and dT phases, and the dT-phase, respectively.

A. Trend of phase transitions

It is well known that the band edge of MX₂ is mainly contribute by the *d*-orbitals of the M atoms[1,41]. An analysis of the energy level splitting of M *d*-orbitals is helpful for exploring the mechanism of phase transitions. The crystal field splitting and electron filling of the *d* shells of group VI-B transition metal atoms in different phases are sketched in Fig. 3a. For the H-phase (Mo in trigonal prismatic coordination), the *d* energy levels split into a singlet *a*₁ (low-energy *d*_{z²}), a doublet *e* (medium-energy *d*_{xy}/*d*_{x²-y²}), and a doublet *e*' (high-energy *d*_{yz}/*d*_{xz})[42,43]. While for the T-phase (octahedral coordination), the *d* orbitals split into a low-energy triplet *t*_{2g} and a high-energy doublet *e*_g. For the dT-phase, Mo in a distorted octahedral coordination and also interact (weakly) with two neighboring Mo atoms (the bottom panel of Fig. 3a), so that there is a further splitting within the *t*_{2g}

and e_g levels. Partial orbital occupation of t_{2g} leads not only to the metallic (semimetallic) properties of the T(dT)-phase but also to the structural instability, which explains why the H-phase is more ubiquitous under environmental conditions for most MX_2 . While monolayer MX_2 cannot transform its phase spontaneously under neutral conditions, recent studies have shown that doping electrons (holes) to two dimensional MX_2 may transform it from the H-phase to the dT(T)-phase.[23,33]

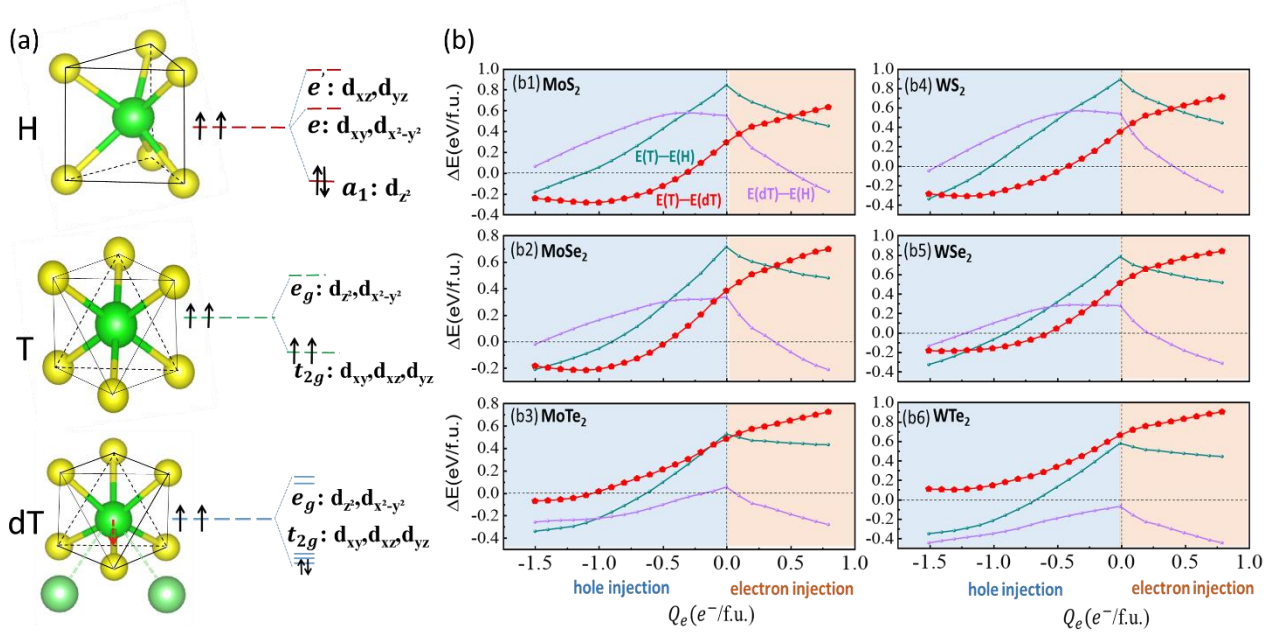


FIG. 3. (a) Coordination, d -levels splitting and electron filling of the transition metal atom of group VIB TMDs in the H-, T- and dT-phase. (b) Energy differences (ΔE) as a function of electron and hole injections between the three phases [$E(T)-E(dT)$, $E(T)-E(H)$ and $E(dT)-E(H)$]. For hole injection, the H-phase transition more efficiently to the metallic T-phase than the semimetallic dT-phase, especially for MoS_2 , WS_2 , MoSe_2 , and WSe_2 .

Fig. 3b shows the energy differences among the three phases [$E(T)-E(dT)$, $E(T)-E(H)$ and $E(dT)-E(H)$] of group VIB MX_2 as a function of electron or hole injection. For electron injection, the $E(dT)-E(H)$ results in Figs. 3b1-b3 reproduces that of the literature[23] well, indicating that our calculation are reliable. Interestingly, Fig. 3b demonstrates that for hole injection, the H-phase transition more efficiently to the metallic T-phase than to the semimetallic dT-phase, especially for MoS_2 , WS_2 , MoSe_2 and WSe_2 . The d -levels splitting and electron filling in Fig. 3a cannot explain this, since it is difficult to distinguish quantitatively between the T and dT phases from crystal field splitting. We then quantify the degree of difficulty of removing (hole injection) or adding electrons (electron injection) from the

three phases by inspecting their ionization energy (IE) or electron affinity energy (EA) for semiconducting H-phase, and work function (WF) for (semi)metallic T and dT phases in Fig. 4 and Fig. S2.

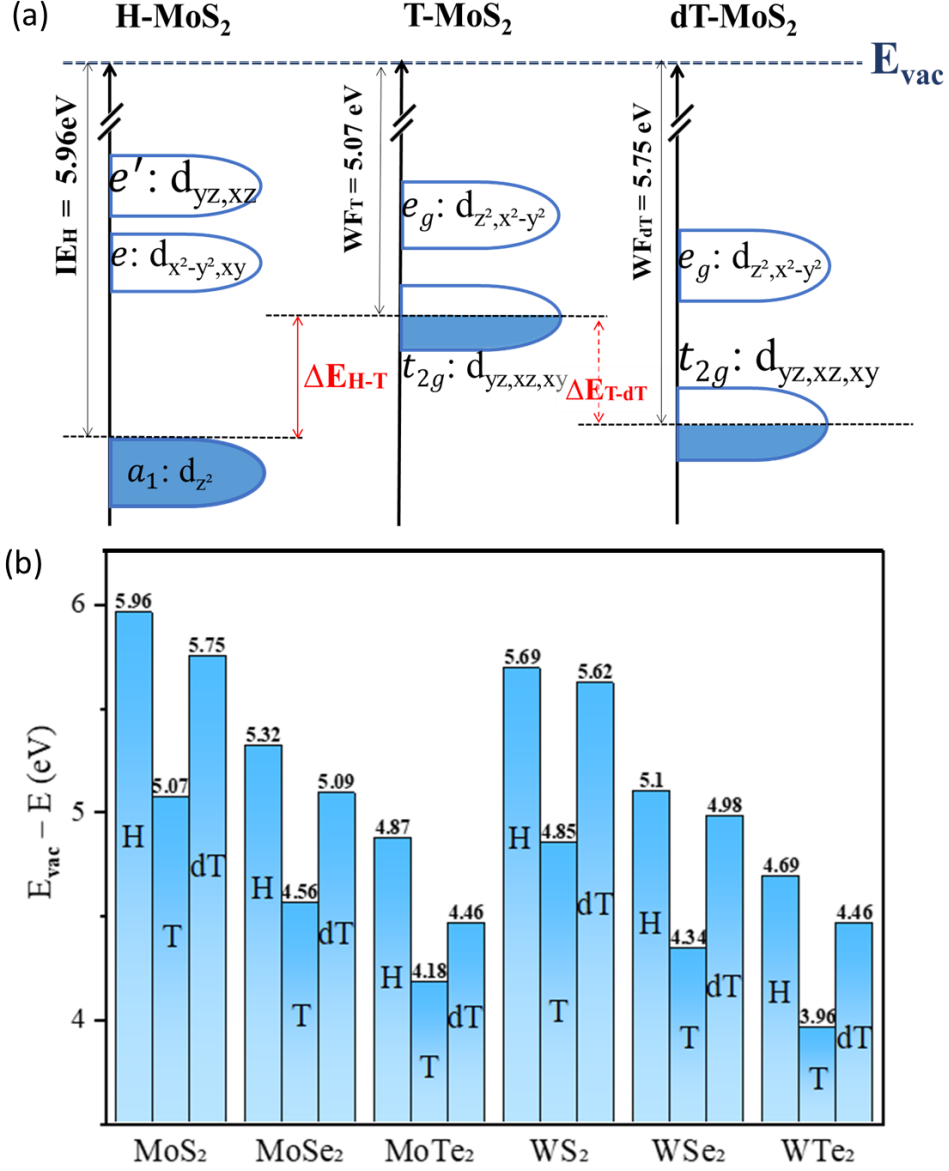


FIG. 4. Ionization energy (IE) of the H-phase and work-function (WF) of the T- and dT-phase of MoS₂ (a) and all group VI-B TMDs (b). It can be seen from (a) that the phase change from H to T is preferred when holes are injected (removing electrons). E_{vac} is the vacuum level.

Taking MoS₂ as an example, Fig. 4a shows that hole-injection (removing electrons) from the H-phase is the most difficult (IE = 5.96 eV), and it is much easier to remove electron from the T-phase

(WF = 5.07 eV) than from the dT-phase (WF = 5.75 eV). Fig. 4b shows that all group VI-B MX₂ in the three phases show the same trend as that of MoS₂, showing that the T-phase is the easiest to remove electrons (hole injection). This explains why in Fig. 3b, the H-phase transition more efficiently to the metallic T-phase than the semimetallic dT-phase for hole injection. Note that, our above analysis can also apply to the H-to-dT phase transition for electron injection, by comparing the EA of the H-phase and the work function of the T and dT phases (Supporting information Fig. S2). So, our method from IE (or EA) and WF analysis has the advantages of quantify the differences between the T and dT phases, and provides a unified understanding to both the electron-induced H-to-dT phase transition and the hole-induced H-to-T phase transition.

Above demonstrates that electron (hole) injection leads to phase transition from the H-phase to the dT(T)-phase, which should not limited to TMDs, but also sheds light on the phase transition of the newly synthesized MSi₂N₄ family (M is a transitional metal)[44,45]. Note that due to the confinement of the outer Si-N layers, only the H and T phases are possible and the dT-phase may not exist in MSi₂N₄[46]. Ding *et al.* reported that the H-phase MSi₂N₄ are only stable for groups V-B and VI-B transition-metal systems, while for the early (groups III-B and IV-B) and late (group VIII-B) transition-metal systems, the T-phase structures are more stable or only the T-phase are stable[47]. This indicate that our conclusion can be applicable to systems beyond TMDs.

B. Heteroatom-doped TMDs

Though it seems that more holes are needed for the T-phase transition than the electrons needed for the dT-phase transition (Fig. 3b), the hole-injection induced T-phase transition has been realized in the experiment[33]. A recent combined experimental and theoretical study by Du *et al.* has shown that the energy difference between the H-phase and T-phase of WS₂ decreases as the yttrium (Y) substitutional doping concentration increase[33]. They found that for the Y concentration of 1/4 the energy difference between T-phase and H-phase reduced to about 0.2 eV, and, with Y, P co-doping the stable phase can be the T-phase under 1/4 Y concentration for the P atom adsorption on top of Y. However, the dT-phase was not considered in their work.

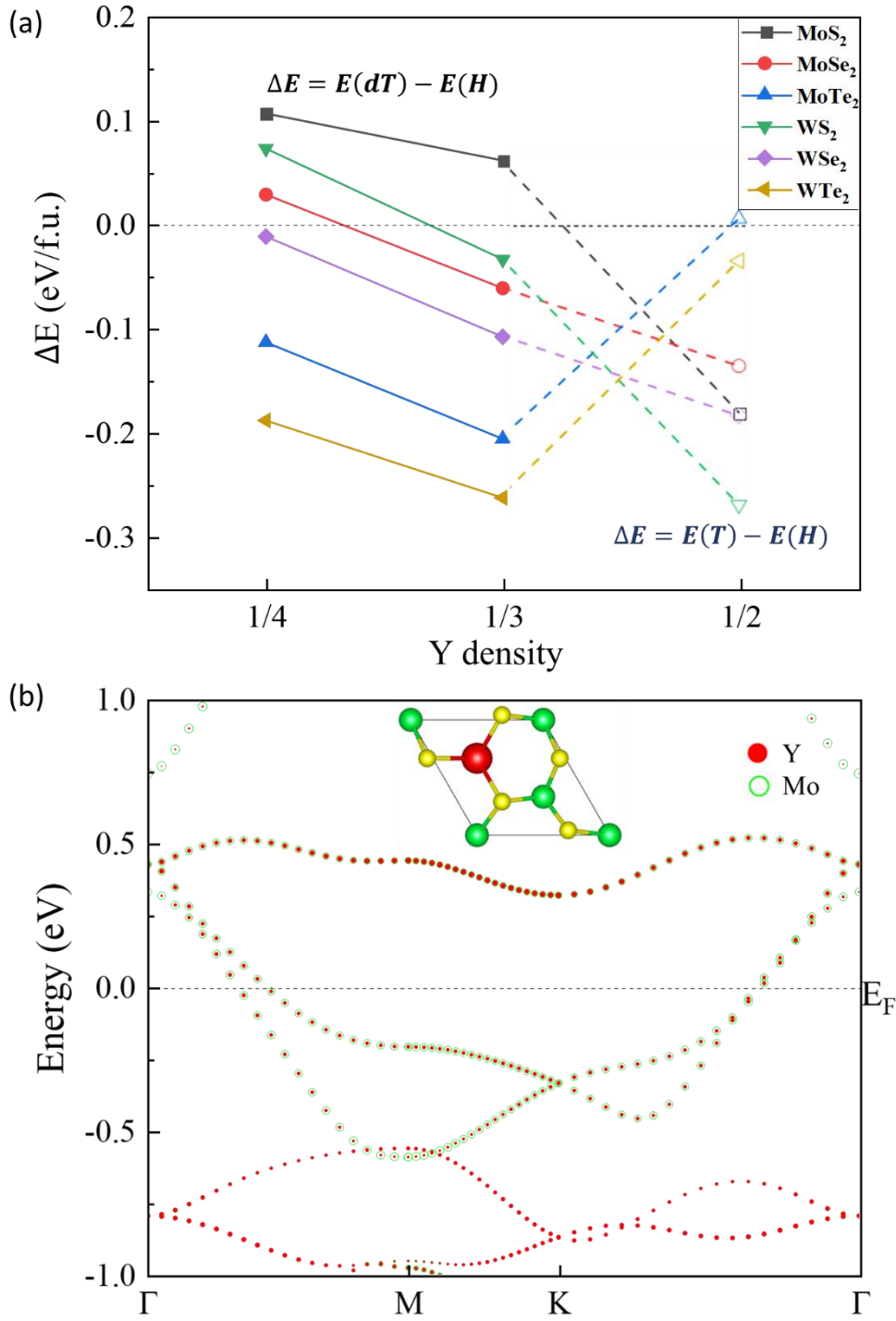


FIG. 5. (a) Energy differences between the H-phase and the dT- or T-phase of group VI-B MX₂ as a function of yttrium (Y) density. For the 1/4 and 1/3 Y concentrations, the dT-phase is more stable than the T-phase and $E(dT)-E(H)$ is shown; while for 1/2 concentration, the T-phase is more stable than the dT-phase and $E(T)-E(H)$ is shown. (b) Projected band structure for 1/3 Y-doped H-MoSe₂. The red and green circles denote the projected band of Y and Mo atoms, respectively.

To consider the possible dT- or T-phase transition from the H-phase with Y doping/alloying, MX_2 with 1/4, 1/3, and 1/2 Y concentrations are considered within $\sqrt{3} \times 2$, $\sqrt{3} \times 3$, and $\sqrt{3} \times 1$ rectangular cells, respectively. We find that Y doping can make the T-phase stable under 1/2 Y concentration (Fig. 5a). Note that in literature[33], Y, P co-doping can obtain the T-phase under 1/4 Y concentration, here we show that Y only may obtain the T-phase with a higher Y concentration. For each Y concentration, all nonequivalent Y substitutional doping patterns are considered, and Fig. 5a shows the lowest energy results. For the 1/4 and 1/3 Y doping concentrations, the dT-phase is more stable than the T-phase and the energy difference of $E(\text{dT})-E(\text{H})$ is shown; while for 1/2 concentration, the T-phase is more stable than the dT-phase and $E(\text{T})-E(\text{H})$ is shown. It is important to note that, under 1/2 Y concentration, the dT-phase cannot exist and relaxed to the T-phase during structural relaxation.

It is interesting to note that in the Y doped systems, a phase transition from H to dT to T occurs (Fig. 5a), the origin (not only hole-doping effect) is beyond the scope of the current work and deserve more detailed study. In addition to complex phase transition, we find that Y-doping may induce the valency change of transition metal Mo and W[48]. For example, for the band structure of H-MoSe₂ with 1/3 Y doping, the energy band of Mo and Y are degenerate and both cross the Fermi level (Fig. 5b). According to our previous study[49], this means that the Mo valency is increased from 4+ to 5+ and the Y valency is 2+, which also confirms that Y doping injects hole into the MoSe₂ system. The same picture applies for Y-doped WS₂ (Fig. S4).

Crystal orbital Hamilton population (*COHP*) bonding analysis and its generalized version, the density of energy (*DOE*) function analysis[38,50], are further performed to understand the phase transitions with increasing Y doping concentration. Taking $(Y_x\text{M}_{1-x})\text{Se}_2$ ($x = 1/3, 1/2$) as examples, the *COHP* curves shows the bonding and antibonding contributions of Y-Se and Mo-Se bonds. Fig. S5 in the Supporting Information shows the *COHP* curve at different Y concentrations of $(Y_x\text{M}_{1-x})\text{Se}_2$. For the H-phase, Y doping induces a large number of anti-bonding states around -5 eV that make the doped system unstable, which is the possible origin for the phase transition. However, for the T-phase, anti-bonding states around -5 eV also appears, although the anti-bonding is weakened near Fermi energy in the doped systems than the undoped one. So, it is difficult to quantify from the *COHP* map. To better quantify the bonding of $(Y_x\text{M}_{1-x})\text{Se}_2$ in the H and T/dT phases, we adopt the density of energy (*DOE*) function[38], which may be seen as the generalized *COHP*:

$$DOE(E) = \sum_k \sum_A \sum_{\mu \in A}^{\mu} \sum_B \sum_{\nu \in B}^{\nu} P_{\mu\nu}(E, k) H_{\mu\nu}(k) \quad (1)$$

The DOE comprises all elements of the density-of-states matrix $P_{\mu\nu}$ and the Hamiltonian matrix $H_{\mu\nu}$, which are made up from the atomic orbitals μ and ν . It sums up all offsite (A-B interatomic) and on-site (intra-atomic) contributions. The entire band energy is given by

$$E_{band} = \int_{-\infty}^{E_F} DOE(E) dE \quad (2)$$

Fig. 6 shows the $DOEs$ and the corresponding band energies (in blue) for the cases with H-to-dT/T phase transitions. The E_{band} value for the dT- or T-phase is always greater than that of the H-phase.

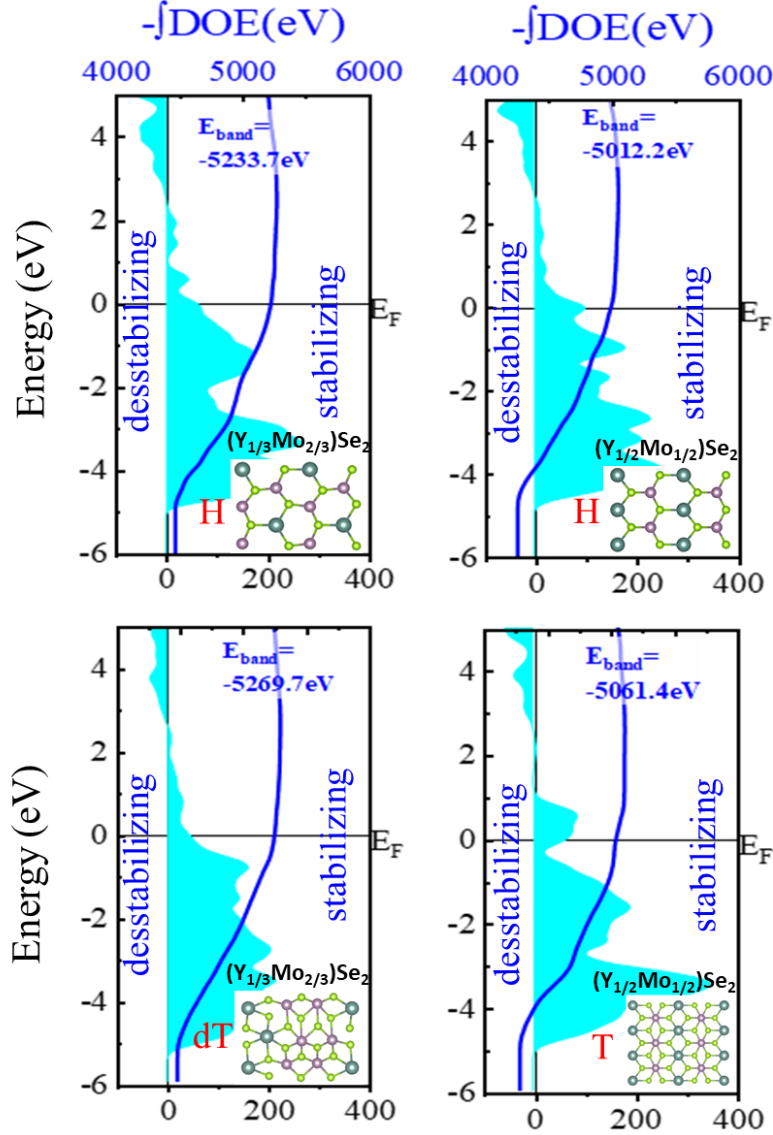


FIG. 6. DOE analysis of the bonding for the cases with H- to dT/T-phase transitions. The DOE energy integrals are shown as blue lines and the total band energy, E_{band} , is also given.

IV. CONCLUSIONS

In conclusion, we performed systematic DFT calculations to obtain a unified understanding to the electron-and hole-driven H-to-dT/T phase transitions in group VI-B monolayer TMDs. Hole injection gives the group VI-B TMDs a phase transition from H to T while electron injection leads a phase transition from H to dT. The origin can be attributed simply to the smaller work function of the T-phase than that of the dT-phase. Our work function analysis can distinguish T and dT phases quantitatively and can give a unified explanation for the phase transitions for both electron doping and hole doping, and is not limited to TMDs. Furthermore, we show that the hole-driven phase transition mechanism can be used to explain the recent experimental observations. Our current work provides a unified understanding of the H-to-T phase transition by hole doping and H-to-dT phase transition by electron doping, and hence helps to expand the possible stable phases of 2D materials.

ACKNOWLEDGMENTS

This work was supported by the Natural Science Foundation of Hebei Province of China (Grants No. A2021201001, A2021201008), the Natural Science Foundation of China (Grants No. 11904154, 12104124, 51772297), the Advanced Talents Incubation Program of the Hebei University (Grants No. 521000981390, 521000981394, 521000981395, 521000981423), and the high-performance computing center of Hebei University.

References

- [1] M. Chhowalla, H. S. Shin, G. Eda, L. J. Li, K. P. Loh, and H. Zhang, The chemistry of two-dimensional layered transition metal dichalcogenide nanosheets, *Nat. Chem.* **5**, 263 (2013).
- [2] T. A. Empante, Y. Zhou, V. Klee, A. E. Nguyen, I. H. Lu, M. D. Valentin, S. A. Naghibi Alvillar, E. Preciado, A. J. Berges, C. S. Merida, M. Gomez, S. Bobek, M. Isarraraz, E. J. Reed, and L. Bartels, Chemical Vapor Deposition Growth of Few-Layer MoTe₂ in the 2H, 1T', and 1T Phases: Tunable Properties of MoTe₂ Films, *ACS Nano* **11**, 900 (2017).
- [3] M. G. Menezes and S. Ullah, Unveiling the multilevel structure of midgap states in Sb-doped MoX₂ (X = S, Se, Te) monolayers, *Phys. Rev. B* **104**, 125438 (2021).
- [4] J. G. Si, W. J. Lu, H. Y. Wu, H. Y. Lv, X. Liang, Q. J. Li, and Y. P. Sun, Origin of the multiple charge density wave order in 1T-VSe₂, *Phys. Rev. B* **101**, 235405 (2020).
- [5] S. Manzeli, D. Ovchinnikov, D. Pasquier, O. V. Yazyev, and A. Kis, 2D transition metal dichalcogenides, *Nat. Rev. Mater.* **2**, 2058 (2017).
- [6] W. Choi, N. Choudhary, G. H. Han, J. Park, D. Akinwande, and Y. H. Lee, Recent development of two-dimensional transition metal dichalcogenides and their applications, *Mater. Today* **20**, 116 (2017).

- [7] A. Wegner, D. Louca, and J. Yang, Local trigonal modes and the suppression of the charge density wave in $\text{TiSe}_{2-x}\text{Te}_x$, *Phys. Rev. B* **99**, 205110 (2019).
- [8] S. Yan, W. Qiao, X. He, X. Guo, L. Xi, W. Zhong, and Y. Du, Enhancement of magnetism by structural phase transition in MoS_2 , *Appl. Phys. Lett.* **106**, 012408 (2015).
- [9] M. Kang, B. Kim, S. H. Ryu, S. W. Jung, J. Kim, L. Moreschini, C. Jozwiak, E. Rotenberg, A. Bostwick, and K. S. Kim, Universal Mechanism of Band-Gap Engineering in Transition-Metal Dichalcogenides, *Nano Lett.* **17**, 1610 (2017).
- [10] D. H. Keum, S. Cho, J. H. Kim, D.-H. Choe, H.-J. Sung, M. Kan, H. Kang, J.-Y. Hwang, S. W. Kim, H. Yang, K. J. Chang, and Y. H. Lee, Bandgap opening in few-layered monoclinic MoTe_2 , *Nature Phys* **11**, 482 (2015).
- [11] Y. Liu, J. Guo, A. Yu, Y. Zhang, J. Kou, K. Zhang, R. Wen, Y. Zhang, J. Zhai, and Z. L. Wang, Magnetic-Induced-Piezopotential Gated MoS_2 Field-Effect Transistor at Room Temperature, *Adv. Mater.* **30**, 1704524 (2018).
- [12] L. H. Fowler-Gerace, D. J. Choksy, and L. V. Butov, Voltage-controlled long-range propagation of indirect excitons in a van der Waals heterostructure, *Phys. Rev. B* **104**, 165302 (2021).
- [13] D. Wickramaratne, M. Haim, M. Khodas, and I. I. Mazin, Magnetism-driven unconventional effects in Ising superconductors: Role of proximity, tunneling, and nematicity, *Phys. Rev. B* **104**, L060501 (2021).
- [14] Y.-C. Wu, T. Taniguchi, K. Watanabe, and J. Yan, Enhancement of exciton valley polarization in monolayer MoS_2 induced by scattering, *Phys. Rev. B* **104**, L121408 (2021).
- [15] Q. H. Wang, K. Kalantar-Zadeh, A. Kis, J. N. Coleman, and M. S. Strano, Electronics and optoelectronics of two-dimensional transition metal dichalcogenides, *Nat. Nanotechnol.* **7**, 699 (2012).
- [16] B. Chen, Y. Meng, J. Sha, C. Zhong, W. Hu, and N. Zhao, Preparation of $\text{MoS}_2/\text{TiO}_2$ based nanocomposites for photocatalysis and rechargeable batteries: progress, challenges, and perspective, *Nanoscale* **10**, 34 (2017).
- [17] K. Wagner, J. Zipfel, R. Rosati, E. Wietek, J. D. Ziegler, S. Brem, R. Perea-Causín, T. Taniguchi, K. Watanabe, M. M. Glazov, E. Malic, and A. Chernikov, Nonclassical Exciton Diffusion in Monolayer WS_2 , *Phys. Rev. Lett.* **127**, 076801 (2021).
- [18] X. Qian, J. Liu, L. Fu, and J. Li, Quantum spin Hall effect in two-dimensional transition metal dichalcogenides, *Science* **346**, 1344 (2014).
- [19] G. Gao, Y. Jiao, F. Ma, Y. Jiao, E. Waclawik, and A. Du, Charge Mediated Semiconducting-to-Metallic Phase Transition in Molybdenum Disulfide Monolayer and Hydrogen Evolution Reaction in New $1T'$ Phase, *J. Phys. Chem. C* **119**, 13124 (2015).
- [20] S. Cho, S. Kim, J. H. Kim, J. Zhao, J. Seok, D. H. Keum, J. Baik, D.-H. Choe, K. J. Chang, K. Suenaga, S. W. Kim, Y. H. Lee, and H. Yang, Phase patterning for ohmic homojunction contact in MoTe_2 , *Science* **349**, 625 (2015).
- [21] H. Shu, F. Li, C. Hu, P. Liang, D. Cao, and X. Chen, The capacity fading mechanism and improvement of cycling stability in MoS_2 -based anode materials for lithium-ion batteries, *Nanoscale* **8**, 2918 (2016).
- [22] F. Xiong, H. Wang, X. Liu, J. Sun, M. Brongersma, E. Pop, and Y. Cui, Li Intercalation in MoS_2 : In Situ Observation of Its Dynamics and Tuning Optical and Electrical Properties, *Nano Lett.* **15**, 6777 (2015).
- [23] X. Zhou, H. Shu, Q. Li, P. Liang, D. Cao, and X. Chen, Electron-injection driven phase transition in two-dimensional transition metal dichalcogenides, *J. Mater. Chem. C* **8**, 4432 (2020).
- [24] C. Zhang, K. C. Santosh, Y. Nie, C. Liang, W. G. Vandenberghe, R. C. Longo, Y. Zheng, F. Kong, S. Hong, R. M. Wallace, and K. Cho, Charge Mediated Reversible Metal-Insulator Transition in Monolayer MoTe_2 and $\text{W}_x\text{Mo}_{1-x}\text{Te}_2$ Alloy, *ACS Nano* **10**, 7370 (2016).
- [25] S. Song, D. H. Keum, S. Cho, D. Perello, Y. Kim, and Y. H. Lee, Room Temperature Semiconductor-Metal Transition of MoTe_2 Thin Films Engineered by Strain, *Nano Lett.* **16**, 188 (2016).
- [26] J. Yuan, Y. Chen, Y. Xie, X. Zhang, D. Rao, Y. Guo, X. Yan, Y. P. Feng, and Y. Cai, Squeezed metallic droplet with tunable Kubo gap and charge injection in transition metal dichalcogenides, *Proc. Natl. Acad. Sci. U.S.A.* **117**, 6362 (2020).
- [27] Y.-C. Lin, D. O. Dumcenccon, Y.-S. Huang, and K. Suenaga, Atomic mechanism of the semiconducting-to-metallic phase transition in single-layered MoS_2 , *Nat. Nanotechnol.* **9**, 391 (2014).

- [28] K.-A. N. Duerloo and E. J. Reed, Structural Phase Transitions by Design in Monolayer Alloys, *ACS Nano* **10**, 289 (2016).
- [29] K. Zhang, B. M. Bersch, J. Joshi, R. Addou, C. R. Cormier, C. Zhang, K. Xu, N. C. Briggs, K. Wang, S. Subramanian, K. Cho, S. Fullerton-Shirey, R. M. Wallace, P. M. Vora, and J. A. Robinson, Tuning the Electronic and Photonic Properties of Monolayer MoS₂ via In Situ Rhenium Substitutional Doping, *Adv. Funct. Mater.* **28**, 1706950 (2018).
- [30] K. Zhang, D. D. Deng, B. Zheng, Y. Wang, F. K. Perkins, N. C. Briggs, V. H. Crespi, and J. A. Robinson, Tuning Transport and Chemical Sensitivity via Niobium Doping of Synthetic MoS₂, *Adv. Mater. Interfaces* **7**, 2000856 (2020).
- [31] P. Rajak, A. Krishnamoorthy, A. Nakano, P. Vashishta, and R. Kalia, Structural phase transitions in a MoWSe₂ monolayer: Molecular dynamics simulations and variational autoencoder analysis, *Phys. Rev. B* **100**, 014108 (2019).
- [32] W. Jin, T. Schiros, Y. Lin, J. Ma, R. Lou, Z. Dai, J.-X. Yu, D. Rhodes, J. T. Sadowski, X. Tong, T. Qian, M. Hashimoto, D. Lu, J. I. Dadap, S. Wang, E. J. G. Santos, J. Zang, K. Pohl, H. Ding, J. Hone, L. Balicas, A. N. Pasupathy, and R. M. Osgood, Jr., Phase transition and electronic structure evolution of MoTe₂ induced by W substitution, *Phys. Rev. B* **98**, 144114 (2018).
- [33] Z. Du, S. Yang, S. Li, J. Lou, S. Zhang, S. Wang, B. Li, Y. Gong, L. Song, X. Zou, and P. M. Ajayan, Conversion of non-van der Waals solids to 2D transition-metal chalcogenides, *Nature* **577**, 492 (2020).
- [34] Blochl, Projector augmented-wave method, *J. Phys. Condens. Matter* **50**, 17953 (1994).
- [35] Kresse and Furthmuller, Efficient iterative schemes for ab initio total-energy calculations using a plane-wave basis set, *J. Phys. Condens. Matter* **54**, 11169 (1996).
- [36] A. A. Adllan and A. DalCorso, Ultrasoft pseudopotentials and projector augmented-wave data sets: application to diatomic molecules *J. Phys. Condens. Matter* **23**, 0953 (2011).
- [37] M. C. Payne, T. A. Arias, and J. D. Joannopoulos, Iterative minimization techniques for ab initio total-energy calculations: molecular dynamics and conjugate gradients, *Rev. Mod. Phys.* **64**, 1045 (1992).
- [38] M. Kupers, P. M. Konze, S. Maintz, S. Steinberg, A. M. Mio, O. Cojocaru-Miredin, M. Zhu, M. Muller, M. Luysberg, J. Mayer, M. Wuttig, and R. Dronskowski, Unexpected Ge-Ge Contacts in the Two-Dimensional Ge₄Se₃Te Phase and Analysis of Their Chemical Cause with the Density of Energy (DOE) Function, *Angew. Chem. Int. Ed. Engl.* **56**, 10204 (2017).
- [39] K.-A. N. Duerloo, Y. Li, and E. J. Reed, Structural phase transitions in two-dimensional Mo- and W-dichalcogenide monolayers, *Nat. Commun.* **5**, 4214 (2014).
- [40] Y. Shi, H. Li, and L.-J. Li, Recent advances in controlled synthesis of two-dimensional transition metal dichalcogenides via vapour deposition techniques, *Chem. Soc. Rev.* **44**, 2744 (2015).
- [41] R. Lv, J. A. Robinson, R. E. Schaak, D. Sun, Y. Sun, T. E. Mallouk, and M. Terrones, Transition Metal Dichalcogenides and Beyond: Synthesis, Properties, and Applications of Single- and Few-Layer Nanosheets, *Acc. Chem. Res.* **48**, 56 (2015).
- [42] C. Gong, H. Zhang, W. Wang, L. Colombo, R. M. Wallace, and K. Cho, Band alignment of two-dimensional transition metal dichalcogenides: Application in tunnel field effect transistors, *Appl. Phys. Lett.* **103**, 053513 (2013).
- [43] X. Ding, S. Zhang, M. Zhao, Y. Xiang, K. H. L. Zhang, X. Zu, S. Li, and L. Qiao, NbS₂: A Promising p-Type Ohmic Contact for Two-Dimensional Materials, *Phys. Rev. Appl.* **12**, 064061 (2019).
- [44] A. Bafekry, M. Faraji, A. A. Ziabari, M. M. Fadlallah, C. V. Nguyen, M. Ghergherehchi, and S. A. H. Feghhi, A van der Waals heterostructure of MoS₂/MoSi₂N₄: a first-principles study, *New J. Chem.* **45**, 8291 (2021).
- [45] Y.-L. Hong, Z. Liu, L. Wang, T. Zhou, W. Ma, C. Xu, S. Feng, L. Chen, M.-L. Chen, D.-M. Sun, X.-Q. Chen, H.-M. Cheng, and W. Ren, Chemical vapor deposition of layered two-dimensional MoSi₂N₄ materials, *Science* **369**, 670 (2020).
- [46] L. Wang, Y. Shi, M. Liu, A. Zhang, Y.-L. Hong, R. Li, Q. Gao, M. Chen, W. Ren, H.-M. Cheng, Y. Li, and X.-Q. Chen, Intercalated architecture of MA₂Z₄ family layered van der Waals materials with emerging topological, magnetic and superconducting properties, *Nat. Commun.* **12**, 2361 (2021).
- [47] Y. Ding and Y. Wang, Computational Exploration of Stable 4d/5d Transition-Metal MSi₂N₄ (M = Y-Cd and Hf-Hg) Nanosheets and Their Versatile Electronic and Magnetic Properties, *J. Phys. Chem. C* **125**, 19580 (2021).
- [48] M. C. Lucking, J. Bang, H. Terrones, Y.-Y. Sun, and S. Zhang, Multivalency-Induced Band Gap Opening at MoS₂ Edges, *Chem. Mater.* **27**, 3326 (2015).

- [49] Y. Ren, Y. Hu, L. Hu, Y. Chen, L. Huang, and X. Shi, Mo-edge reconstructions in MoSe₂ and MoS₂: Reexamination of the mechanism, *Phys. Rev. B* **104**, 115406 (2021).
- [50] V. L. Deringer, W. Zhang, M. Lumeij, S. Maintz, M. Wuttig, R. Mazzarello, and R. Dronskowski, Bonding nature of local structural motifs in amorphous GeTe, *Angew. Chem. Int. Ed. Engl.* **53**, 10817 (2014).